Contents lists available at ScienceDirect

## Geochimica et Cosmochimica Acta

journal homepage: www.elsevier.com/locate/gca



## Thallium isotope cycling between waters, particles, and sediments across a redox gradient



Chadlin M. Ostrander <sup>a,b,c,\*</sup>, Sune G. Nielsen <sup>b,d</sup>, Hayley J. Gadol <sup>e</sup>, Luciana Villarroel <sup>a,f</sup>, Scott D. Wankel <sup>a</sup>, Tristan J. Horner <sup>a,b</sup>, Jerzy Blusztajn <sup>b,d</sup>, Colleen M. Hansel <sup>a</sup>

- <sup>a</sup> Department of Marine Chemistry and Geochemistry, Woods Hole Oceanographic Institution, Woods Hole, MA, USA
- <sup>b</sup> NIRVANA Laboratories, Woods Hole Oceanographic Institution, Woods Hole, MA, USA
- <sup>c</sup> Department of Geology and Geophysics, University of Utah, Salt Lake City, UT, USA
- <sup>d</sup> Department of Geology and Geophysics, Woods Hole Oceanographic Institution, Woods Hole, MA, USA
- <sup>e</sup> Department of Civil and Environmental Engineering, Massachusetts Institute of Technology, Cambridge, MA, USA
- Department of Earth, Atmospheric and Planetary Sciences, Massachusetts Institute of Technology, Cambridge, MA, USA

#### ARTICLE INFO

#### Article history: Received 23 November 2022 Accepted 22 March 2023 Available online 28 March 2023 Associate editor: Caroline P. Slomp

Keywords: Paleoredox Trace elements Brackish Manganese Euxinic

#### ABSTRACT

Thallium (Tl) isotopes are an emerging tool for tracking the history of molecular oxygen in seawater. Use of TI isotopes in this manner requires a thorough understanding of the modern TI isotope cycle, especially within the anoxic settings that typified Earth's past oceans. To this end, we generated Tl concentration and isotope data for waters, particles, and sediments collected during three spring-summer-fall field seasons in Siders Pond, a salt-stratified and sulfide-rich ('euxinic') pond on Cape Cod (Massachusetts, USA). Over short timeframes (i.e., days to weeks), we observed a large degree of variability in the abundance  $(Tl_{diss} = 9 \text{ pM} - 42 \text{ pM})$  and isotopic composition ( $\varepsilon^{205}Tl_{diss} = -3.9 \pm 0.4$ ; 2SD to  $-0.1 \pm 0.7$ ; 2SD) of dissolved Tl in pond surface waters. Thallium drawdown was common and favored removal of the lighter-mass Tl isotope. We surmise that biological Tl uptake plays a role in this phenomenon, but more work is warranted to confirm this hypothesis. Manganese oxides persisted in pond surface waters on many sampling days but had no obvious effect on  $Tl_{diss}$ , only a slight effect on particulate  $\epsilon^{205}Tl$  values on the day of most prolific Mn oxide accumulation (driving  $\epsilon^{205}Tl_{part}$  as high as  $+0.9\pm0.8$ ; 2SD). In euxinic waters below the oxycline, rapid drawdown of dissolved Tl was observed on all sampling days together with a complimentary increase in particulate Tl (up to Tl<sub>part</sub> = 21 pM). Strong associations between Tl and sulfide, and between Tl and other chalcophile metals (Mo and Cd), suggest that Tl is probably removed from euxinic waters in association with particulate sulfides, and seemingly with no resolvable isotopic fractionation effect despite non-quantitative TI removal. The sediment data track the longer-term TI cycle in the pond (i.e., across years) and reveal limited isotopic variability. Thallium isotope compositions leached from surface sediments match those predicted for contemporaneous waters, or nearly so, at all depths in the pond (above, within, and below the oxycline). Apparently, only a small fraction of the short-term Tl isotope variability found in the oxic surface waters of Siders Pond gets transferred to anoxic waters, and essentially none is transferred to sediments. Our results reaffirm the notion that Tl isotopes are uniquely capable of tracking long-term sedimentary Mn oxide burial - not mere Mn oxide formation. Our results also verify the ability of sediments formed under reducing conditions to capture the Tl isotope composition of contemporaneous waters. More broadly, the results of our investigation bolster our knowledge of the modern Tl isotope cycle and thereby permit more confident inferences of this cycle in Earth's past.

© 2023 Elsevier Ltd. All rights reserved.

# \* Corresponding author at: Department of Geology and Geophysics, University of

Utah, Salt Lake City, UT, USA.

E-mail address: chadlin.ostrander@utah.edu (C.M. Ostrander).

## 1. Introduction

Interest in the post-transition metal thallium (Tl) is growing among geochemists. Thallium is a generally conservative element in the ocean today (Flegal and Patterson, 1985) and highly toxic (Zitko, 1975). Yet, transient non-conservative Tl behavior was

recently observed in the North Sea (Böning et al., 2018), and this behavior is linked, rather surprisingly, to biological uptake by phytoplankton (Mori et al., 2021a, 2021b). Thallium has a strong affinity for Mn(IV)-bearing oxide minerals (referred to henceforth as Mn oxides; Hein and Koschinsky, 2014), and at least some Mn oxides possess a strong preference for the heavier-mass Tl isotope (205Tl; Peacock and Moon, 2012; Nielsen et al., 2013). Manganese oxides are unstable under reducing conditions (reduction leads to mobilization as soluble Mn(II/III); Froelich et al., 1979; Madison et al., 2013), and so their survival in sediments today occurs exclusively in locations where molecular oxygen (O<sub>2</sub>) persists at the sediment–water interface (Calvert and Pedersen, 1996).

This indirect link to O2 has thrust Tl isotopes into the role of burgeoning paleoredox proxy. Manganese oxides are ubiquitous on the well-oxygenated seafloor today, and their preferential removal of <sup>205</sup>Tl drives the globally homogenous seawater Tl isotope composition ( $\varepsilon^{205}$ Tl) to a value lower than global marine inputs (seawater  $\epsilon^{205}$ Tl = -6.0 ± 0.3 compared to an input value of  $\varepsilon^{205}$ Tl  $\approx$  -2; Nielsen et al., 2017). In contrast, sediments formed today under reducing conditions do not fractionate Tl isotopes, leading to capture of the overlying seawater  $\epsilon^{205}$ Tl value. These findings form the basic premise of the Tl isotope paleoredox proxy: seawater  $\epsilon^{205}$ Tl values can be reconstructed from ancient sedimentary rocks formed under reducing conditions and used to indirectly track changes in past marine O<sub>2</sub> levels by tracking changes in past seafloor Mn oxide burial. At times when Earth's oceans became better oxygenated, expanded seafloor Mn oxide burial should have resulted in a lower seawater  $\varepsilon^{205}$ Tl value (e.g., during the late-Archean; Ostrander et al., 2019). At times of expanded marine anoxia, contracted seafloor Mn oxide burial should have resulted in a higher seawater  $\varepsilon^{205}$ Tl value (e.g., during Mesozoic Oceanic Anoxic Events; Ostrander et al., 2017; Them et al., 2018; Wang et al., 2022a).

From out of this growing interest a need arises to better understand how Tl and its two stable isotopes, <sup>203</sup>Tl and <sup>205</sup>Tl, are cycled in nature. Strides are being made on this topic (summarized in Nielsen et al., 2017), but one barrier that remains difficult to breach is the extremely low dissolved Tl abundances (Tl<sub>diss</sub>) found in some bodies of water, particularly those that are anoxic. Below the oxycline in the Cariaco Basin and Black Sea, Tl<sub>diss</sub> is observed as low as 6.8 pM and 1.6 pM, respectively (Owens et al., 2017), or roughly 1 ng Tl  $L^{-1}$ . Generation of accurate and precise Tl isotope ratio data generally requires at least a few nanograms of Tl under typical analysis conditions (Nielsen et al., 2004). Hence, the collection and purification of many liters of anoxic waters is oftentimes required in order to generate reliable Tl isotope data for these sample types. As a result, dissolved Tl isotope data are currently only available for two anoxic water column samples (immediately below the oxycline in the Black Sea; Owens et al., 2017). And, to our knowledge, there are no published particulate Tl isotope data whatsoever for particles formed in or delivered to anoxic waters.

The currently coarse data resolution from anoxic settings leads to many knowledge gaps in our understanding of how Tl and its isotopes are cycled in these environments. These gaps set critical limitations on our ability to reconstruct ancient marine redox using Tl isotopes because anoxic conditions typified Earth's oceans for most of geologic time (Lyons et al., 2021). For example, to what extent do short-term oscillations in Mn oxide production impact sedimentary Tl isotope compositions? What fractionation is observed during Tl co-precipitation with sulfides under anoxic conditions? And does biological uptake of Tl impart any detectable isotope fractionation in environmental settings?

To help fill these and other knowledge gaps, we studied the cycling of Tl and its isotopes during three spring-summer-fall field seasons in Siders Pond, a salt-stratified body of water with strong redox zonation located on Cape Cod (Massachusetts, USA). We pre-

sent new Tl abundance and isotopic data for waters and particles collected on multiple days from the oxic and anoxic and sulfiderich ('euxinic') portions of the water column. On select days, these Tl data are complemented by trace metal and Mn oxide data. We also present data for surface sediments collected along a shallow-to-deep transect. Our dataset provides new insights into how Tl and its isotopes are cycled between waters, particles, and sediments under variable redox conditions in a natural setting, revealing a high degree of short-term spatial variability in waters and particles that largely evades preservation over longer time-scales in the sedimentary record.

#### 2. Study site and sample collection

#### 2.1. Siders Pond

Siders Pond is a small coastal meromictic kettle hole (volume =  $10^6$  m³, area = 13.4 ha, maximum depth = 15 m) located in downtown Falmouth, Massachusetts, on Cape Cod (Fig. 1). The pond is estimated to receive about  $1\times10^6$  m³ of freshwater and  $0.15\times10^6$  m³ of saltwater annually (Caraco, 1986). Freshwater enters the pond via rain, storm water runoff from downtown Falmouth, and a culvert connecting Siders Pond to neighboring Shivericks Pond. Seawater enters the pond through a small waterway referred to as "fresh river" that connects the pond to Vineyard Sound about 550 m to the south. Fresh surface and salty deep waters in the pond do intermix; however, regular subsurface seawater input, and subsequent dilution by fresh surface waters, has been hypothesized to sustain the strong density stratification and prevent collapse of the salt gradient (Caraco, 1986).

Siders Pond is strongly salt-stratified and thus meromictic. The lack of vertical mixing drives persistent redox stratification; dissolved oxygen (DO) contents are high in fresh surface waters (exceeding 10 mg/L), but rapidly decline and are replaced by anoxic waters below about five meters depth (with some temporal and spatial variability; Figs. 2 and 3). Deeper, saltier anoxic waters are enriched in hydrogen sulfide (up to 8 mM during sampling, again with some temporal and spatial variability; Figs. 2 and 3).

Samples were collected over seven days during the 2019, 2020, and 2021 spring–summer–fall field seasons. Siders Pond was accessed via an inflatable dinghy equipped with an electric motor, oftentimes with the support of a paddle canoe. The dinghy was anchored at approximately the same site on all sampling days, at the southward end of the pond above a deep sampling site (approximate 11.5 m deep; Fig. 1). Before any samples were collected, a YSI multi-probe system (556 MPS) was deployed to characterize the basic structure of the pond on that sampling day (e.g., pH, salinity, DO). A lone surface-water sample from Shivericks Pond was collected on July 31, 2021 just north of Katharine Lee Bates Road, at the mouth of a culvert that runs below downtown Falmouth connecting the upstream Shivericks to Siders Pond.

#### 2.2. Water collection

All waters were collected by pumping water through Norprene tubing (MasterFlex) from desired depths via a peristaltic pump directly into acid-cleaned bottles. Before sampling each depth, sufficient water was pumped through the tubing to flush water collected at the previous depth. For the purposes of generating Tl abundance data, 15 to 50 mL of water was collected from each depth, filtered (see the next sub-section), and acidified to 0.1 M HCl, from which a small aliquot was taken for measurement ( $\sim$ 150 uL on average). For the purposes of generating Tl isotope ratio data, the amount of water collected at each depth was much

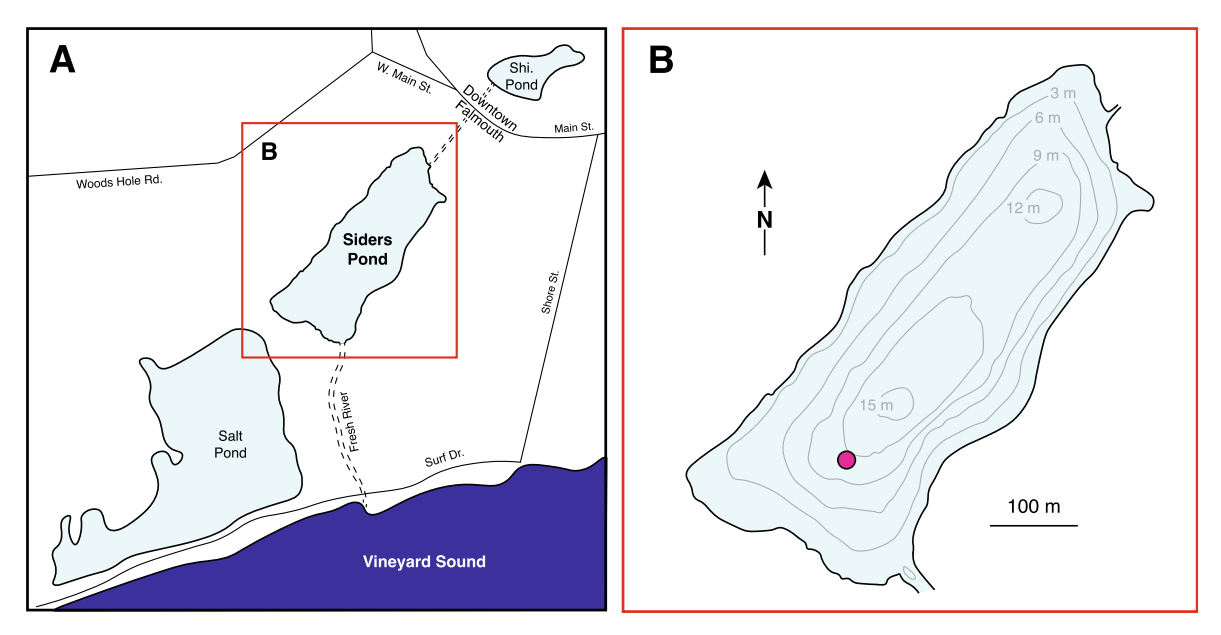


**Fig. 1. (A)** Location of Siders Pond (Cape Cod, USA). **(B)** Bathymetry map reconstructed from Caraco (1986). The magenta circle marks the location of dissolved and particulate water sample collection. (For interpretation of the references to color in this figure legend, the reader is referred to the web version of this article.)

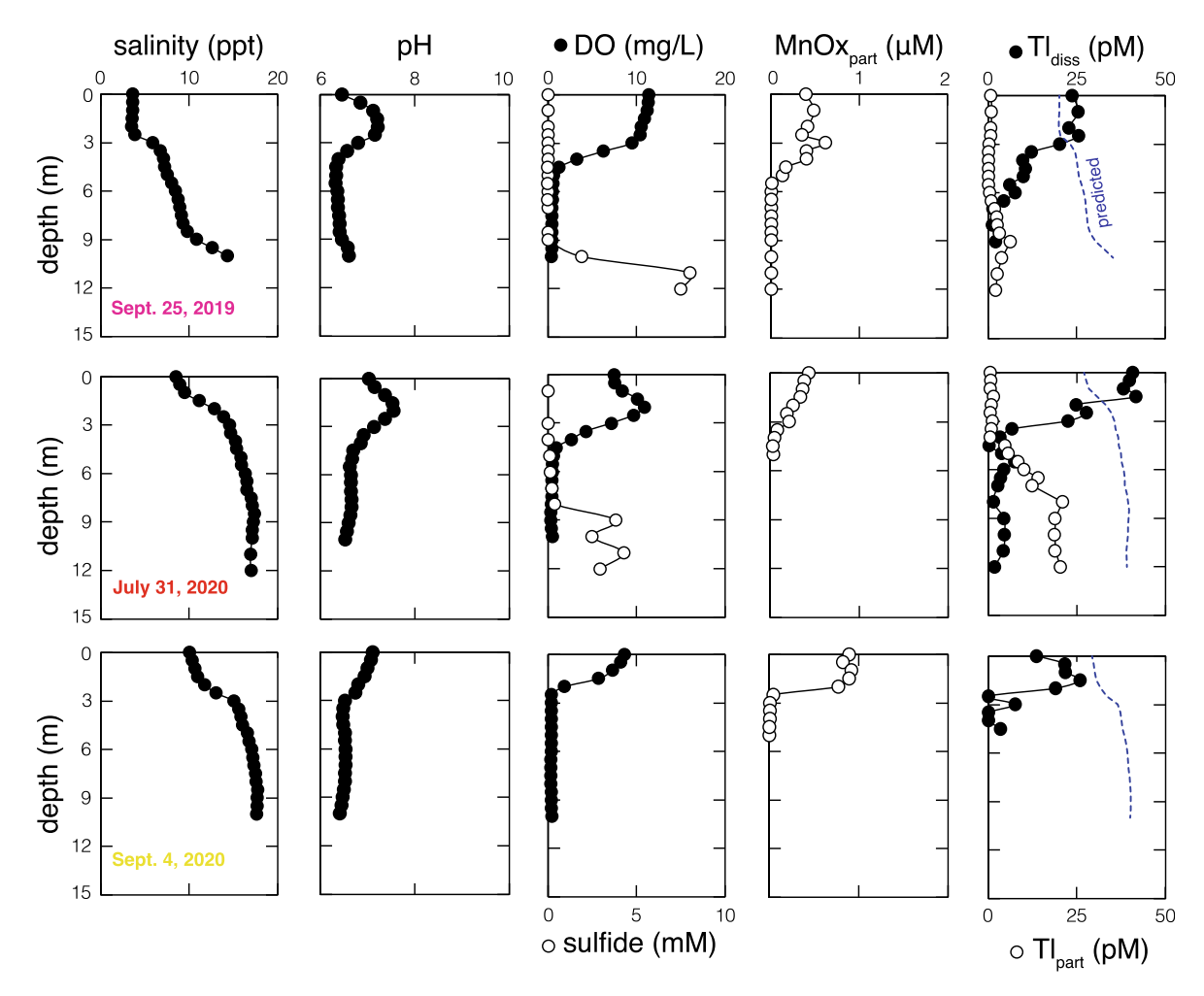


**Fig. 2.** Data collected from Siders Pond. Filled circles signify dissolved data and unfilled circles signify particulate data, with the exception of the sulfide data which come from unfiltered waters. See methods for an explanation of error bars. "Predicted" line is calculated assuming a conservative distribution and two-component freshwater-seawater mixing (see Section 5.1).

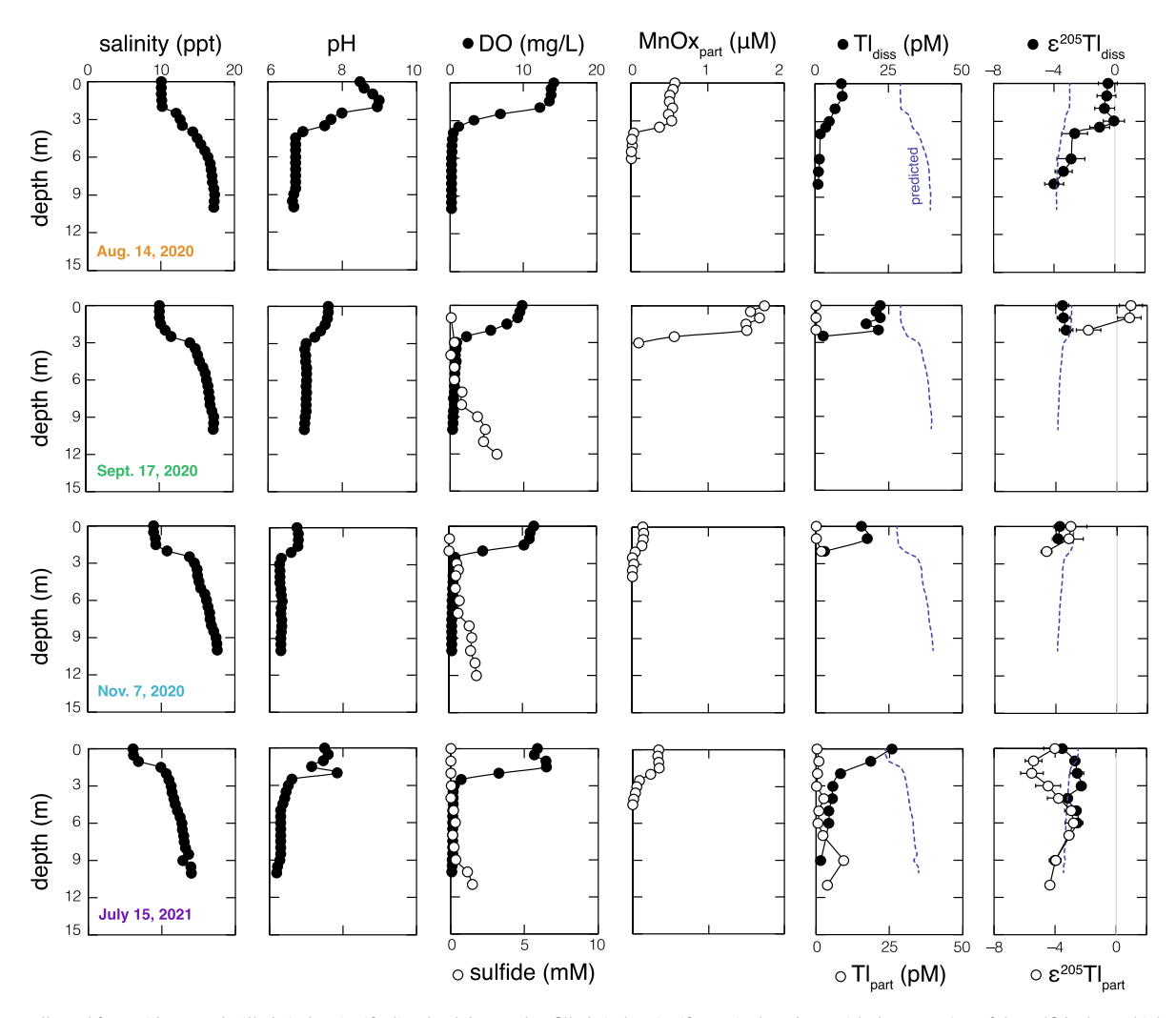


**Fig. 3.** Data collected from Siders Pond. Filled circles signify dissolved data and unfilled circles signify particulate data, with the exception of the sulfide data which come from unfiltered waters. See methods for an explanation of error bars. "Predicted" lines are calculated based on salinity assuming a conservative distribution and two-component freshwater-seawater mixing (see Section 5.1).

greater and varied between 0.5 L and 10 L, the goal being to collect  $\geq$  0.5 ng of Tl for isotopic analyses.

#### 2.3. Particle collection

For the purposes of quantifying particulate Mn oxide contents, 0.22  $\mu m$  pore size Sterivex polyethersulfone (PES) filter cartridges (Millipore) were attached directly to the ends of the *peri*-pump tubing with a luer lock fitting. For each sample, a known volume typically between 100 mL and 250 mL was passed through a Sterivex filter. Filters were put on ice and placed in a freezer as soon as was possible after collection, always within a few hours.

Polyethersulfone membrane filters (Millipore), also 0.22 μm pore size, were used for the purposes of obtaining particulate Tl data. All PES membrane filters, and associated filter hardware, were cleaned following the procedures outlined in Cutter et al. (2017). When the goal was to generate only Tl abundance data, 50 mL of water from each depth was loaded into a syringe in the field and passed through a 25 mm PES membrane filter housed inside a filter holder (Swinnex, Millipore). When the goal was to generate Tl isotope data, this method was up-scaled and moved to WHOI to account for the much larger sample volumes. Each head on a six-position Advantec PVC vacuum manifold was equipped with a 500 mL Nalgene funnel. A 47 mm PES membrane filter was then placed inside each Nalgene funnel. One-by-one,

each large-volume water sample was pulled by vacuum through this filter rig. Filters were replaced as needed until filtering was complete for the sample, and then the rig was cleaned in preparation for the next sample.

After filtering, all PES membrane filters were transferred to perfluoroalkoxy alkane (PFA) vials (Savillex) and constituted in 0.6 M hydrochloric acid (HCl) at a scaling of 2.5 mL per cm² of filter area. Each vial was then placed overnight on a hot plate at 80 °C to leach particulate materials (after Bishop et al., 2012). After filter leaching, filters were carefully removed from PFA vials with plastic tweezers. Each sample was then digested using a series of concentrated acid mixtures. The first acid mixture was a 1:1 mixture of concentrated HCl and concentrated nitric acid (HNO<sub>3</sub>), a step that was repeated until no solid material was visible. This was followed by a  $\sim 10:1$  mixture of concentrated HNO<sub>3</sub> and hydrogen peroxide (H<sub>2</sub>O<sub>2</sub>) to dissolve organics, a step that was repeated until samples no longer stuck to the interior walls of the PFA vials. Hydrofluoric acid (HF) was not used at any time during particle digestion in order to avoid dissolution of lithogenic silicates.

## 2.4. Sediment collection

Only on two days during the 2020 field season were sediments collected from the pond. On both days, we sampled a shallow-to-deep transect moving toward (and in the case of one especially

deep sample, past) the site targeted for water and particle sample collection. Initially (Aug. 20, 2020), a Van Veen dredge was used to collect material present at and immediately below the sedimentwater interface. This method proved to be challenging, however, as cobbles and boulders were abundant close to shore (preventing collection of any sediment) and sediments from deeper portions of the pond were extremely soft (hampering the trigger mechanism). Only four sediment samples were successfully collected using the Van Veen dredge. We achieved a much higher success rate by collecting sediments directly through the tubing (Sept. 4, 2020); tubing was lowered to the bottom of the pond and solid materials were pumped to the surface in a slurry. By employing this sampling method, we understand that we are getting only a broad picture of the sediments, homogenized over a few centimeters depth and the unknown timeframe this represents.

After collection, a sub-sample was taken from each wet sediment sample and placed in a PFA vial for drying. Samples were dried on a hot plate at 50 °C over the course of a week. Once completely dry, each sample was ground into a fine powder using a pestle and mortar. The pestle and mortar were cleaned between samples with water and then ethanol, followed by grinding with Sigma-Aldrich white quartz sand (≥99.995 trace metal basis). Once powdered, each sample was transferred to a trace metal clean screw top bottle.

To generate bulk-sediment trace metal abundance data, a small amount of powder from each sample, about 20 mg, was transferred to a PFA vial and digested to completion using the same acid mixtures described above for the particles. Only a slight modification was made to the first mixture, whereby concentrated HF was added to the 1:1 mixture of HNO<sub>3</sub> and HCl to help digest any silicates in the bulk-sediments. For sedimentary Tl isotopes, a slightly larger amount of powder from each sample, about 100 mg, was transferred to a PFA vial and subjected to an overnight 2 M HNO<sub>3</sub> leach shown in previous work to successfully isolate authigenic TI from detrital TI (Nielsen et al., 2011; Owens et al., 2017). Pyrite is the primary carrier of this authigenic Tl when sediments form under reducing conditions (Nielsen et al., 2011), although some role could also be reserved for earlier formed and less stable iron-sulfide phases (e.g., iron monosulfides; future work should explore this possibility). After leaching, samples were centrifuged in trace metal clean centrifuge tubes, with the supernatant being pipetted into a new PFA vial and serving as the "authigenic" split, and the remaining solid material being transferred back into the original PFA vial and serving as the "detrital" split. Each of these splits was then digested to completion, again using the same acid mixtures as described above for the other solid samples. In the case of the detrital splits, HF was once again added to the first mixture to aide in silicate digestion.

## 3. Analytical methods

## 3.1. Trace element data

Trace element concentration data were generated using a Thermo Fisher Scientific iCAP Q Inductively Coupled Plasma Mass Spectrometer (ICPMS) located at the WHOI Plasma Mass Spectrometry Facility. Concentrations were calculated via reference to ion beam intensities obtained from a five-point calibration curve constructed from serial dilutions of a gravimetrically prepared multielement standard. Each sample was doped with indium (In) before measurement, and drift was monitored and corrected for by normalizing to In intensities. Accuracy and precision of similar concentration measurements on the same instrument have been

determined to be ±5–10% (1SD) based on agreement with USGS reference materials AGV-1, AGV-2, BHVO-1, BHVO-2, BIR-1, and BCR-2 that were treated as unknowns during earlier runs (Jochum et al., 2016; Shu et al., 2017).

#### 3.2. Particulate Mn oxide data

Most of the particulate Mn oxide data discussed herein is reported previously by Gadol (2021). Only a few new data are reported here, and these data were generated using the same methodologies employed in Gadol (2021). Briefly, particulate Mn oxide abundances (pMnOx) were quantified using the leucoberbelin blue (LBB) assay with a permanganate standard curve (Altmann, 1972; Oldham et al., 2015). Sterivex cartridge filters containing pond particles were filled with 2 mL LBB at a concentration of 0.004% in 0.1% acetic acid and then sealed with Parafilm. After approximately two hours, the liquid extract was removed and absorbance was measured at 620 nm on a UV–Vis spectrophotometer.

## 3.3. Thallium isotope data

Before Tl isotope analysis, all samples were purified from matrix elements in the NIRVANA Laboratory using previously established techniques (Rehkämper and Halliday, 1999; Nielsen et al., 2004; Owens et al., 2017). For digested particle and sediment samples, each was constituted in 5 mL 1 M HCl, amended with brominated water, and passed through a glass column packed with 1.5 mL of AG1-X8 anion exchange resin. For acidified water samples, each was amended with brominated water and passed through a large-volume glass column (~600 mL) manufactured specifically to account for the large sample volumes (again, between 0.5 L and 10 L). After the initial glass column, all samples were constituted in a small volume  $\sim$ 9:1 mixture of concentrated HNO<sub>3</sub> and hydrogen peroxide (H<sub>2</sub>O<sub>2</sub>) to dissolve any organics eluted from the column. Thereafter, this purification step was repeated using a second, much smaller Teflon micro-column packed with 0.1 mL of the same resin, followed by another round of digestion with HNO<sub>3</sub> and H<sub>2</sub>O<sub>2</sub> before final constitution in 0.1 M HNO<sub>3</sub> plus 0.1% sulfuric acid in preparation for isotope ratio measurement.

Thallium isotope ratio measurements were performed using a Thermo Finnigan Neptune multi-collector ICPMS (MC-ICPMS) located at the WHOI Plasma Mass Spectrometry Facility. An Aridus II desolvating nebulizer system was used during sample introduction. Measurements were performed in low-resolution mode using sample-standard bracketing and external normalization to NIST SRM 981 Pb. The Tl isotope compositions are reported relative to NIST SRM 997 in epsilon notation:

$$\epsilon^{~205} Tl = \left( ~^{205/203} Tl_{sample} / ~^{205/203} Tl_{NIST-997} - 1 \right) \times 10,000.$$

Because the ion exchange separation procedure returns 100% yields (Rehkämper and Halliday, 1999; Nielsen et al., 2004) and each sample was doped with a known quantity of NIST SRM 981 Pb, Tl concentrations could be calculated during MC-ICPMS analysis using measured <sup>205</sup>Tl/<sup>208</sup>Pb ratios.

Thallium isotope ratio measurements of modern and ancient marine sedimentary rocks have become routine in the NIRVANA Lab over the past half-decade. Sediment splits and standards were analyzed at a concentration of  $\sim$ 7 ng/g Tl, which typically yielded an ion current around 80 pA on m/z 205 ( $10^{11}~\Omega$  resistor). All sediment splits were analyzed in duplicate. The average and maximum 2 standard deviation (SD) reproducibility of these duplicate measurements was 0.1 and 0.3 epsilon units for the authigenic

splits and 0.4 and 0.7 epsilon units for the detrital splits. One USGS shale SCo-1 standard was leached, purified, and analyzed with each sediment sample set to monitor accuracy. This standard yielded an authigenic  $\epsilon^{205}\text{Tl}$  value (henceforth  $\epsilon^{205}\text{Tl}_A$ ) of  $-3.0\pm0.2$ ; 2SD and a detrital  $\epsilon^{205}\text{Tl}$  value (henceforth  $\epsilon^{205}\text{Tl}_D$ ) of  $-2.7\pm0.4$ ; 2SD, both of which are indistinguishable from values reported in previous work ( $\epsilon^{205}\text{Tl}_A=-2.9\pm0.1$ ; 2SD and  $\epsilon^{205}\text{Tl}_D=-2.5\pm0.3$ ; 2SD; Ostrander et al., 2017). Reported error for our sediment splits are always in 2SD and either equal to the reproducibility of the respective SDO-1 split or the individual sample's reproducibility, whichever is greater.

Generating Tl isotope data for waters and particles was comparatively difficult because of the low Tl contents of these sample types. Most particle and water samples (15 of 16 and 20 of 24, respectively) were analyzed only once, and at ion currents as low as 4 pA (m/z 205). To monitor the reproducibility of samples measured only once and at such low ion currents, an Aldrich Tl standard solution and a dissolved TICl solution were analyzed during the same analytical sessions at comparable ion currents. Under typical analytical conditions (7 ng/g Tl solution yielding an ion current of  $\sim$ 80 pA on m/z 205), the Aldrich and TlCl solutions yielded indistinguishable  $\varepsilon^{205}$ Tl values, averaging  $-0.7 \pm 0.3$ ; 2SD (n = 16). Previous analyses of the Aldrich standard solution over the course of 20+ years reveal the same value, averaging -0.8 ± 0.4; 2SD (n = 187; Nielsen et al., 2017). When these Aldrich and TlCl solutions yielded ion currents between 3 pA and 10 pA, the average  $\varepsilon^{205}$ Tl value was  $-0.8 \pm 1.1$ ; 2SD (n = 10), reproducible within error of the same value measured under typical analytical conditions but with a lower precision. When analyzed at slightly higher ion currents between 10 pA and 20 pA, the average  $\varepsilon^{205}$ Tl value for these solutions was  $-0.6 \pm 0.4$ ; 2SD (n = 5), which was in much better agreement with the same value measured under typical analytical conditions. If this improvement in precision arises solely from counting statistics, the trend should follow a power law with an exponent of -0.5. Such a trend is indeed observed (Fig. 4) and is consistent with other Tl isotope studies that collected data at low ion beam intensities (Nielsen et al., 2007, 2015). For particle and water samples measured only once, associated 2SD uncertainties are estimated using the relationship in Fig. 4. Reported uncertainties for the few water (n = 4) and particle (n = 1) samples measured in duplicate are either equal to the highest 2SD reproducibility of the Aldrich and TlCl solutions analyzed under typical analytical conditions (0.3 epsilon units) or the individual sample's reproducibility, whichever is greater.

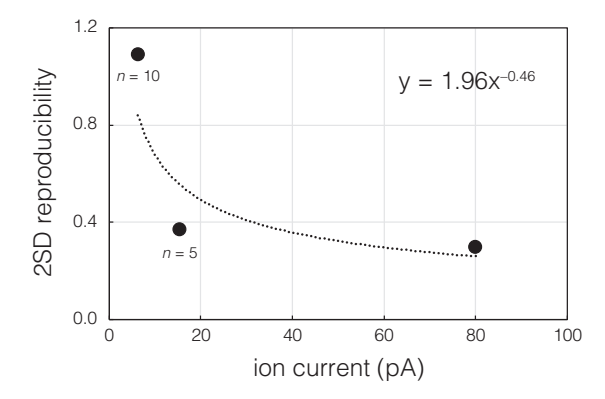


**Fig. 4.** The 2SD reproducibility of Tl isotope standard solutions analyzed at low ion currents (in epsilon notation) plotted versus the average ion current for that solution. The resultant power law is used to calculate a 2SD for particle and water samples measured only once and at comparable ion currents.

#### 4. Results

#### 4.1. Water column results

Maximum dissolved Tl abundances ( $Tl_{diss}$ ) in fresh  $O_2$ -bearing surface waters varied over the three-year study period, ranging 9–42 pM (Figs. 2 and 3). However, a fairly restricted range of maximum  $Tl_{diss}$  between 22 pM and 26 pM was found on four out of the seven sampling days (Sept. 25, 2019; Sept. 4, 2020; Sept. 17, 2020; July 15, 2021). On the day when surface  $Tl_{diss}$  was particularly low (Aug. 14, 2020), surface pH reached a value of 9, which was considerably higher than on any other sampling day (pH never exceeded 8 on any other day).

Dissolved Tl abundances decreased in saltier anoxic deep waters on all sampling days (Figs. 2 and 3). On some days, Tl<sub>diss</sub> decreased rapidly below a single depth at or near the oxycline (e.g., Aug. 14, 2020). On other days, Tl<sub>diss</sub> decreased in stages at multiple depths, slightly above or at the oxycline and below it (e.g., Sept. 25, 2019 and July 15, 2021). Maximum Tl<sub>diss</sub> in salty deeper waters spanned a range between 1 pM and 10 pM, averaging 6 pM.

A wide range of dissolved Tl isotope compositions ( $\epsilon^{205}\text{Tl}_{\text{diss}}$ ) was observed in fresh surface waters, from as low as  $-3.9 \pm 0.4$  to as high as  $-0.1 \pm 0.7$  (Fig. 3). The highest surface  $\epsilon^{205}\text{Tl}_{\text{diss}}$  values were observed on the day when pH reached 9, the same day maximum Tl<sub>diss</sub> in surface waters reached only 9 pM (Aug. 14, 2020).

A comparatively muted range of  $\epsilon^{205} Tl_{diss}$  values was observed in salty deep waters. Deep pond waters were collected for the purposes of generating  $\epsilon^{205} Tl_{diss}$  data on only two days and revealed indistinguishable ranges between  $-4.0 \pm 0.6$  and  $-2.9 \pm 0.9$  (Aug. 14, 2020) and between  $-4.0 \pm 0.4$  and  $-2.3 \pm 0.3$  (July 15, 2020) (Fig. 3).

A lone water sample collected from Shivericks Pond on July 31, 2021 yielded a Tl<sub>diss</sub> of 15 pM and a  $\epsilon^{205}$ Tl<sub>diss</sub> value of  $-1.8 \pm 0.4$ .

## 4.2. Particulate results

Particulate Tl abundances ( $Tl_{part}$ , calculated relative to filtered water volumes) were persistently low in fresh surface waters, spanning a range between 0.1 pM and 1.9 pM (Figs. 2 and 3). On days when  $Tl_{part}$  data were generated for surface waters and deep waters,  $Tl_{part}$  increased with depth. The depth in the water column at which this  $Tl_{part}$  increase occurred varied between days, from as shallow as 4.5 m (July 31, 2020) to as deep as 7 m (Sept. 25, 2019). Deeper water  $Tl_{part}$  were especially high on July 31, 2020, peaking at 21 pM. Compare this to maximum  $Tl_{part}$  of 6.3 pM on Sept. 25, 2019 and 9.4 pM on July 15, 2021. This day of peak  $Tl_{part}$  was also the day of peak  $Tl_{diss}$  in surface waters.

Particulate  $\epsilon^{205}TI$  values ( $\epsilon^{205}TI_{part}$ ) were highly variable between sampling days in fresh surface waters, from as low as  $-5.5 \pm 0.7$  to as high as  $+0.9 \pm 0.8$  (Fig. 3). Interestingly, particles possessed higher  $\epsilon^{205}TI$  values than coeval waters on one day (up to  $\epsilon^{205}TI_{part} - \epsilon^{205}TI_{diss} = +4.5$  on Sept. 17, 2020) and lower  $\epsilon^{205}TI$  values on another (down to  $\epsilon^{205}TI_{part} - \epsilon^{205}TI_{diss} = -3.0$  on July 15, 2021). On the day when we observed higher  $\epsilon^{205}TI_{part}$  than in coeval waters, we also observed the highest particulate MnOx contents (up to MnOx<sub>part</sub> = 1.7  $\mu$ M). On the day when we observed lower  $\epsilon^{205}TI_{part}$  than coeval surface waters, we also observed a sharp decline in  $TI_{diss}$  with depth in these same surface waters.

A muted range of  $\epsilon^{205} Tl_{part}$  was observed for the few samples collected from the anoxic deep saltier portion of the pond on July 15, 2021, from as low as  $-4.4 \pm 0.3$  to as high as  $-2.8 \pm 0.6$  (Fig. 3). None of these  $\epsilon^{205} Tl_{part}$  was distinguishable outside of error from coeval waters.

On the two days for which we generated a suite of particulate trace element data (Sept. 25, 2019 and July 31, 2020)  $Tl_{part}$  were strongly correlated with Mo<sub>part</sub> abundances ( $R^2 \geq 0.8; \ Fig. 5A$ ). On one of these days (July 31, 2020) a strong correlation was also found between  $Tl_{part}$  and  $Cd_{part}$  ( $R^2$  = 0.9).

## 4.3. Sediment results

Authigenic Tl abundances ( $Tl_A$ ) leached from bulk-sediments span a wide range, from as low as 34 ng/g to as high as 1,548 ng/g (Fig. 6A). The lowest  $Tl_A$  were found in sediments underlying fresh surface waters, and particularly within the oxycline. The highest  $Tl_A$  were found in sediments underlying anoxic deep saltier waters, with a single sediment sample collected

8.5 m below the pond surface having a much higher abundance than the others. Sediment materials that did not dissolve during the leach step (referred to henceforth as the "detrital" fraction, or  $\text{Tl}_D$ ) revealed lower and comparatively less variable Tl abundances between 14 ng/g and 167 ng/g (Fig. 6C). The lowest  $\text{Tl}_D$  was found in the sediment sample collected one meter below the pond surface, whereas the highest  $\text{Tl}_D$  was found in the same 8.5 m sample with an especially high  $\text{Tl}_A$  abundance. Of the total Tl in each bulk-sediment sample, most was present within the authigenic fraction ( $f_A$ ) at the surface and below the oxycline, whereas most Tl was present within the detrital fraction ( $f_D$ ) across the oxycline (Fig. 6B).

Authigenic Tl isotope compositions ( $\epsilon^{205}$ Tl<sub>A</sub>) gradually decreased with distance from shore, starting at  $-2.8 \pm 0.3$  beneath

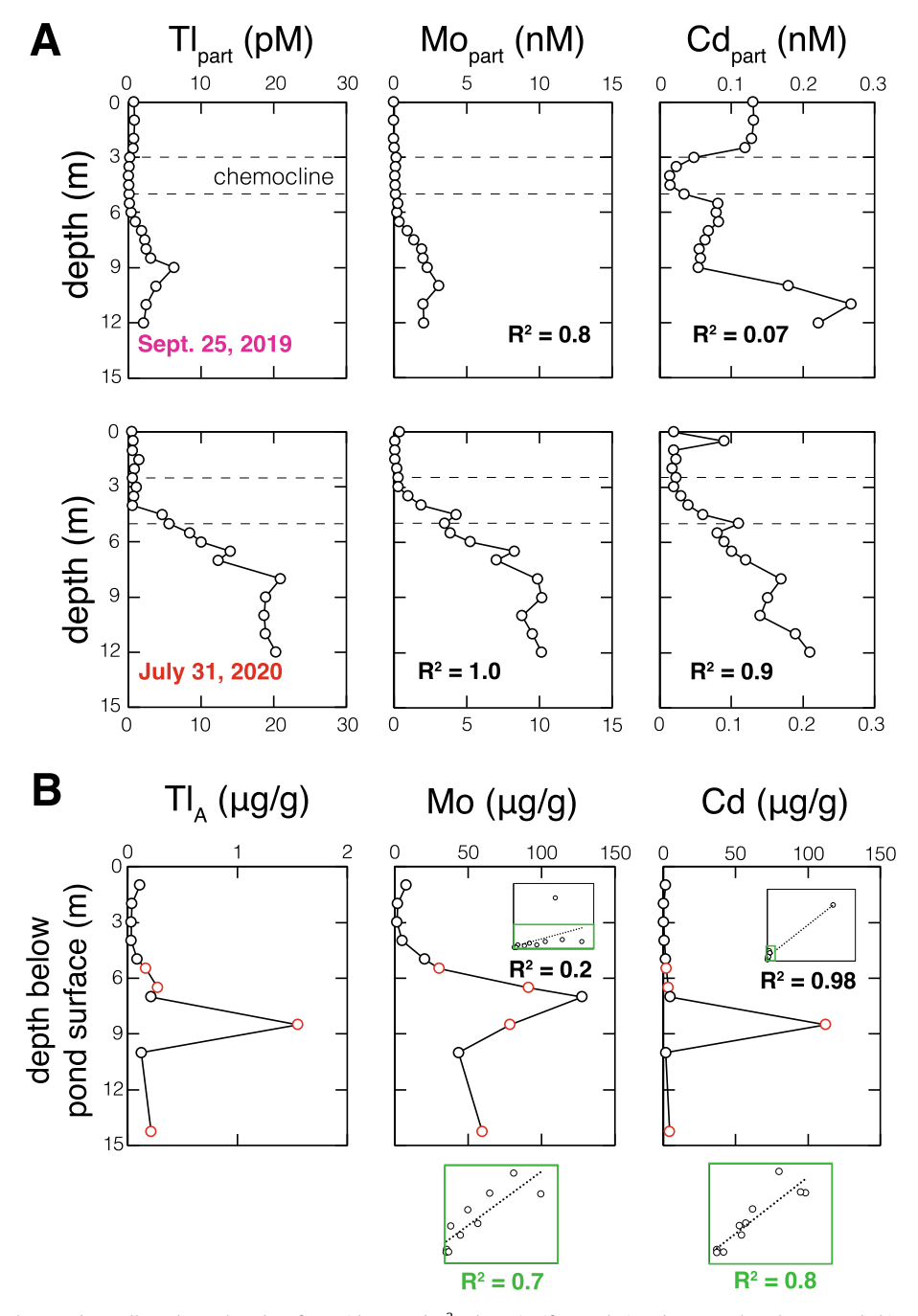


**Fig. 5.** (A) Particulate trace element data collected on select days from Siders Pond. R<sup>2</sup> values signify correlations between that element and Tl in particles. (B) Sediment trace metal data collected from Siders Pond. Cross-plots located within the panels signify Tl correlations using all sediment data (Tl = y-axis, Mo/Cd = x-axis). Cross-plots located below the panels signify Tl correlations when excepting the lone sediment sample with an especially strong Tl enrichment.

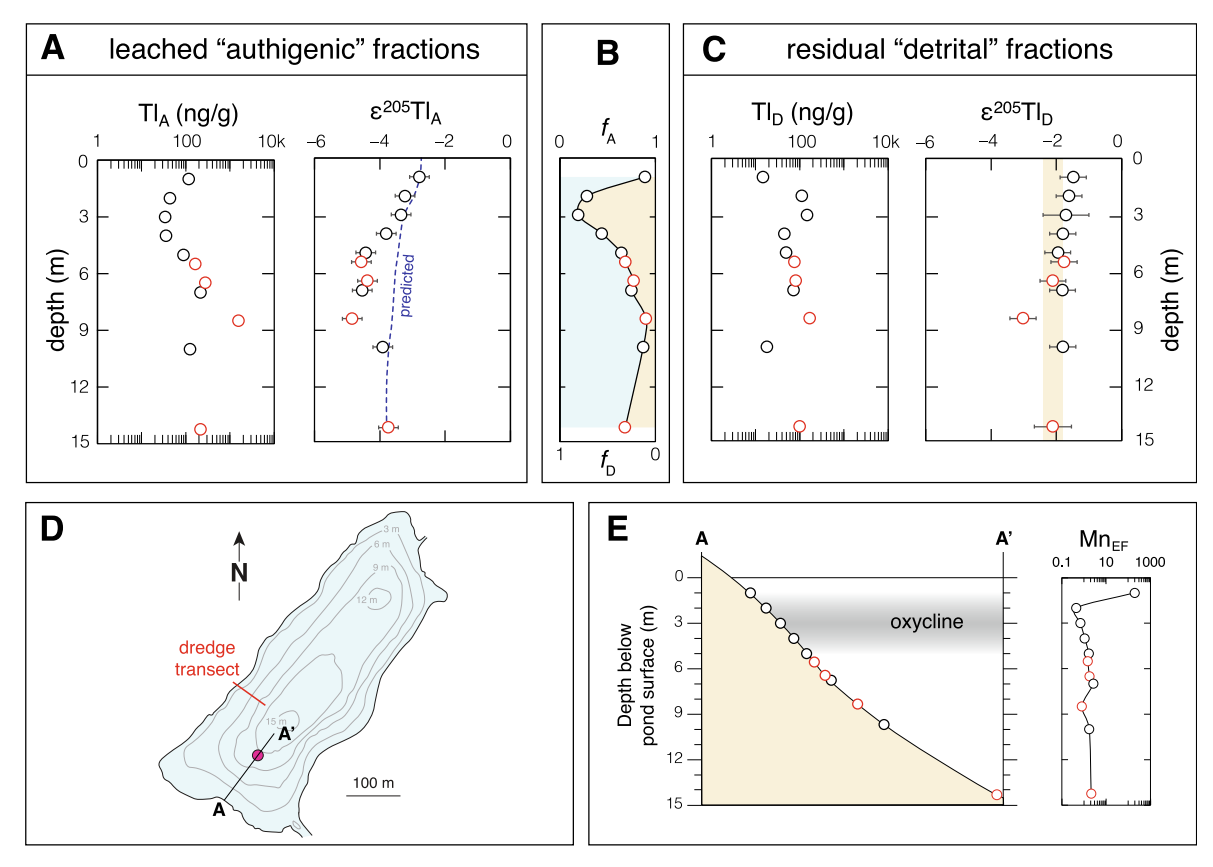


**Fig. 6.** (A) 'Authigenic' Tl abundance and isotope data leached from sedimentary pyrite. "Predicted" line is calculated based on average salinity of contemporaneous waters assuming a conservative distribution and two-component freshwater-seawater mixing (see Section 5.1). (B) Relative fraction of the total bulk-rock Tl concentration contained in the authigenic ( $f_A$ ; blue) and detrital ( $f_D$ ; brown) sample fractions. (C) 'Detrital' Tl abundance and isotope data left behind in the solid residue after the pyrite leach. The brown shaded region signifies modern bulk upper continental crust. (D) Sediment transect paths. (E) Bathymetry map. The x-axis is to scale but the y-axis has been expanded to accentuate depth. Black unfilled datapoints come from sediment samples collected via peristaltic pump and red unfilled datapoints come from sediment samples collected via dredge. (For interpretation of the references to color in this figure legend, the reader is referred to the web version of this article.)

fresh surface waters and reaching a nadir of  $-4.8 \pm 0.3$  at 8.5 m (Fig. 6A). Below this nadir, sediments collected from the two deepest points in the pond at 10 m and 14.25 m reveal a slight but noticeable shift to higher  $\epsilon^{205} Tl_A$  of  $-3.9 \pm 0.3$  and  $-3.7 \pm 0.3$ . Detrital Tl isotope compositions ( $\epsilon^{205} Tl_D$ ) are generally invariant (Fig. 6C), with one sole datapoint being distinguishable from the estimated average of bulk upper continental crust ( $\epsilon^{205} Tl_{BUCC} = -2.1 \pm 1.0$ ; Nielsen et al., 2017). The exceptional datapoint is, once again, found at 8.5 m below the pond surface and reaches  $-3.0 \pm 0.4$ .

Trace element data were also generated for bulk-sediments, revealing an especially strong correlation between  $Tl_A$  and Cd ( $R^2$  = 0.98; Fig. 5B). If the 8.5 m sediment sample with an especially high  $Tl_A$  concentration is excluded, a strong correlation is also found between  $Tl_A$  and Mo ( $R^2$  = 0.7). The sedimentary  $Tl_A$ -Cd correlation is subdued but still present when the 8.5 m datapoint is excluded ( $R^2$  = 0.8). Manganese enrichment factors (Mn\_{EF}, where Mn\_{EF} = Mn/Al $_{\rm sample}$   $\div$  Mn/Al $_{\rm bulk-crust}$  using bulk crust estimates from Rudnick and Gao, 2003) were fairly low in all samples collected below one meter water depth (average Mn\_{EF} = 1.43). The sediment sample from one meter water depth had an especially high Mn\_{EF} of 199 (Fig. 6E).

## 5. Discussion

We discuss the Tl cycle in Siders Pond beginning with fresh surface waters (Section 5.1.) before moving to deeper salty waters (Section 5.2.) and then pond sediments (Section 5.3.). In the final

section, we discuss the implications of our results for the Tl isotope paleoredox proxy (Section 5.4).

## 5.1. Thallium cycling in fresh oxic surface waters

A reasonable assumption is that binary mixing of freshwater and seawater governs the distribution of Tl and its isotopes within Siders Pond. Armed with the Tl concentration and isotope composition of these two end-members and their respective salinities, we constructed a predicted profile of Tl<sub>diss</sub> and  $\epsilon^{205} \text{Tl}_{diss}$  in pond waters for each day based on the salinity profile and assuming conservative mixing. For these predictions, we assume a seawater end-member equivalent to the open ocean (salinity = 35 ppt, Tl<sub>diss</sub> = 65 pM, and  $\epsilon^{205} \text{Tl}_{diss}$  = -6.0; Owens et al., 2017). For the freshwater end-member, we use data collected from Shivericks Pond (salinity = 0.1, Tl<sub>diss</sub> = 15 pM, and  $\epsilon^{205} \text{Tl}_{diss}$  = -1.8 epsilon units), which receives freshwater runoff from the same (downtown Falmouth) area and directly supplies freshwater to Siders Pond (Fig. 1). All conservative Tl<sub>diss</sub> and  $\epsilon^{205} \text{Tl}_{diss}$  predictions are plotted in Figs. 2 and 3.

#### 5.1.1. Thallium surplus

Only on one sampling day (July 31, 2020) did we measure  $Tl_{diss}$  much higher than predicted based on pond salinity ( $Tl_{diss}$  as high as 42 pM). Particulate Tl abundances in deep waters also peaked on this day, reaching 21 pM below the oxycline. We can think of two possible explanations for this apparent Tl surplus: (1) sedi-

mentary Mn oxide dissolution or (2) a heterogenous mixture of Tl in pond surface waters.

It is possible that reductive dissolution of Mn oxides buried in oxidizing near-shore sediments led to the transient release of Tl to the surface waters of Siders Pond. Thallium has a strong affinity for the surface of manganese oxide minerals (Hein and Koschinsky, 2014), and reductive dissolution of these minerals upon contact with anoxic waters would be expected to lead to the release of sorbed Tl (Böning et al., 2018; Ahrens et al. 2021). The location of the oxycline did change throughout the course of our study, with some shoaling taking place across the summer-fall transition (apparent in Figs. 2 and 3). Ideally, this hypothesis would be tested with Tl isotopes; Tl released from sedimentary Mn oxides would likely be enriched in the heavier-mass isotope (Nielsen et al., 2013). Surface waters collected two weeks later did have higher  $\epsilon^{205} Tl$  values (up to  $\epsilon^{205} Tl_{diss}$  = -0.1 ± 0.5). However, and on top of the complexities associated with the two-week temporal gap, surface water Tl<sub>diss</sub> on this subsequent sampling day was very low (~9 pM). It therefore seems more likely that this heaviermass Tl isotope enrichment was the consequence of an additional or altogether different process (expanded upon in Section 5.1.2).

Alternatively, it is possible that Tl is heterogeneously distributed in the surface waters of Siders Pond. In this scenario, at least some changes in surface water  $Tl_{diss}$  – and, for that matter, also  $\epsilon^{205}Tl_{diss}$  – were due to spatial differences in the Tl distribution of the pond.

Unfortunately, we cannot confidently differentiate between these two hypotheses using the available data. Instead, we will focus more keenly on the more common phenomenon observed in Siders Pond during our three-year investigation: surface water  $Tl_{\rm diss}$  depletions.

## 5.1.2. Thallium depletion

We observed a strong surface water  $Tl_{diss}$  depletion on one sampling day relative to the conservative mixing predictions (Aug. 14, 2020), and a weaker but nonetheless still noticeable  $Tl_{diss}$  depletion on two additional days (Nov. 7, 2020 and July 15, 2021). We can think of four possible explanations for these depletions: (1) adsorption to Mn oxides, (2) removal by sulfides, (3) biological uptake, or (4) a heterogenous mixture of Tl in pond surface waters. Explanations 1–3 are expanded upon below.

Manganese oxides are shown to form in oxygenated surface waters of Siders Pond (Gadol, 2021), and thus serve as a potential Tl<sub>diss</sub> depletion mechanism. If this were the case, then we would expect to see the preferential removal of the heavier-mass Tl isotope from surface waters on the days of Tl<sub>diss</sub> depletion (Nielsen et al., 2013). However, particles were only found to be distinctly enriched in the heavier-mass Tl isotope relative to coeval waters on Sept. 17, 2020 (up to  $\varepsilon^{205}$ Tl<sub>part</sub> –  $\varepsilon^{205}$ Tl<sub>diss</sub> = +4.5), when surface waters were only mildly Tl-depleted (Fig. 3). This was the same day we found the highest particulate Mn oxide abundances (up to 1.7 µM), and so it seems very likely that some Tl was being removed from surface waters by Mn oxides on this day. However, the remaining, most severe Tl<sub>diss</sub> depletions seem to have been accompanied instead by preferential removal of the lighter-mass Tl isotope. Most directly, particles collected within the oxycline on July 15, 2021 concurrent with a sub-surface Tl<sub>diss</sub> depletion (down from 26 pM at the surface to 6 pM at three meters depth) were enriched in the lighter-mass isotope relative to coeval waters down to  $\varepsilon^{205} \text{Tl}_{part} - \varepsilon^{205} \text{Tl}_{diss} = -3.0$ ; Fig. 3).

Owens et al. (2017) hypothesized that decreasing  $Tl_{diss}$  together with a shift to higher  $\epsilon^{205}Tl_{diss}$  values below the oxycline in the Black Sea ( $\sim$ 2 epsilon units) may have been due to the preferential removal of the lighter-mass Tl isotope during water column pyrite formation. In Siders Pond, decreasing  $Tl_{diss}$  are consistently observed below the oxycline, coincident with an increase in  $Tl_{part}$ 

and sulfide accumulation that likely tracks Tl removal by pyrite (or other metal sulfide phases) at this portion of the water column (see next section). However,  $\epsilon^{205} \text{Tl}$  values generated for particles and waters immediately below the oxycline on July 15, 2021 are indistinguishable, implying little to no isotopic fractionation during Tl removal under euxinic conditions (Fig. 3). Thallium transfer to particles was not quantitative in these waters (only between 14% and 32% of the total Tl at these depths was present in particles), and so any associated isotope fractionation effect should have been visible. Because we did not see any observable sulfide-induced isotopic fractionation in the ideal location of the water column to track this process, we find it difficult to envision such effects taking place higher in the water column under less ideal (oxic) conditions.

Recent experimental studies identified a key role for phytoplankton in removing Tl from surface waters (Zhang and Rickaby. 2020: Mori et al., 2021a, 2021b). The currently favored hypothesis is that Tl(I) is mistakenly taken into cells through K(I) channels (Tl (I) and K(I) have the same ionic charge and similar ionic radii; Tao et al., 2008). Biological uptake oftentimes results in preferential incorporation of the lighter-mass isotope as these isotopes form weaker bonds and are thus easier to break, leaving behind a complementary accumulation of heavier-mass isotopes in solution. This conceptual framework is consistent with the  $\epsilon^{205}$ Tl<sub>part</sub> data collected in surface waters on July 15, 2021, which are lower than coeval waters (Fig. 3). Furthermore, on the sampling day with the strongest surface water Tl<sub>diss</sub> depletion and highest surface water  $\epsilon^{205} Tl_{diss}$  values (Aug. 14, 2020), we also observed the highest pH (up to pH = 9) and DO contents (up to 14 mg/L). This latesummer pH increase, and corresponding supersaturation of  $O_2$ , reflects a peak in surface water productivity (removal of CO<sub>2</sub> from the water column during photosynthesis increases pH), an event that could have increased biological Tl uptake. If, indeed, this process tends to remove the lighter-mass Tl isotope, the mass-balance complement would be enrichment of the heavier-mass Tl isotope in coeval waters.

The isotope fractionation effect imparted during surface water TI removal on August 14, 2020 is estimated in Fig. 7. If Rayleigh fractionation is assumed, the  $\epsilon^{205} Tl_{diss}$  data can be explained by fractionation factors ( $\alpha$ ) from 0.9999 to 0.9997 ( $\alpha_{average}$  = 0.99983). If open-system fractionation at steady state is assumed, these data can be explained by  $\alpha$  ranging from 0.9998 to 0.9996 ( $\alpha_{average}$  = 0.99967). Interestingly, these  $\alpha$  are similar in magnitude to those calculated between univalent TI and univalent TI complexed with three water molecules during mass-dependent and nuclear-volume effects at low temperatures (O °C and 25 °C, where  $\alpha \approx 0.99981$ ; Schauble, 2007). Perhaps this combination of isotope fractionation processes plays some role in driving the observed effects in Siders Pond waters (e.g., uptake of  $^{205}$ TI-depleted TI(I) not complexed to water molecules). Future work should test this hypothesis.

## 5.2. Thallium cycling in salty anoxic deep waters

Compared to surface waters, cycling of Tl and its isotopes in salty, anoxic deep waters seems fairly straightforward. Thallium was rapidly removed from the water column below the oxycline on all sampling days (>5 m depth), resulting in dramatically lower Tl<sub>diss</sub> abundances than predicted with conservative mixing (Tl<sub>diss</sub> – Tl<sub>pred</sub>; summarized in Fig. 8C). Our  $\epsilon^{205}$ Tl<sub>diss</sub> data resolution was much coarser in this portion of the pond, but the data that were generated more closely matched the conservative predictions ( $\epsilon^{205}$ Tl<sub>diss</sub> –  $\epsilon^{205}$ Tl<sub>pred</sub>; Fig. 8D). And we observed no resolvable Tl isotope fractionation between anoxic waters and particles within these waters ( $\epsilon^{205}$ Tl<sub>part</sub> –  $\epsilon^{205}$ Tl<sub>diss</sub>; Fig. 8E).

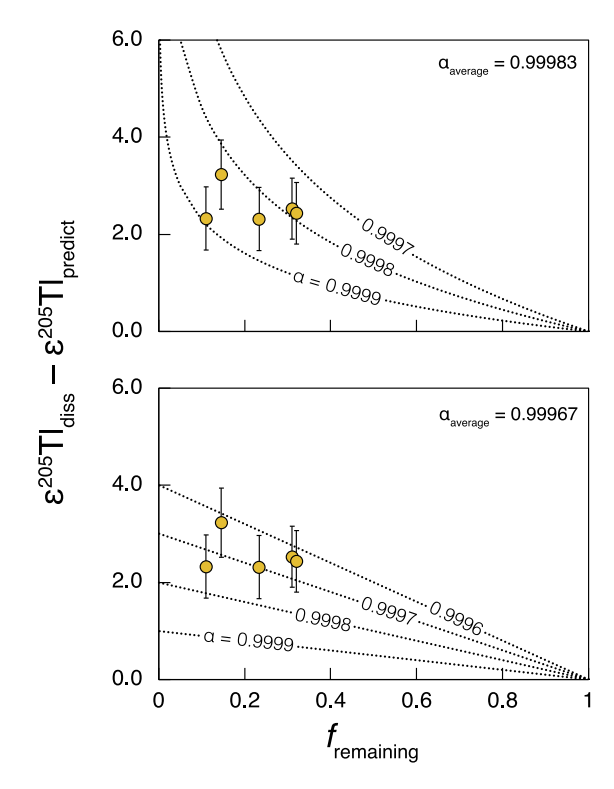


**Fig. 7.** Isotope fractionation factor model results plotted atop Siders Pond surface water data collected August 14, 2020. The Tl isotopic effect and fraction remaining are calculated based on "predicted" values from two-component mixing. The upper panel assumes Rayleigh fractionation, while the lower panel assumes open-system fractionation at steady state.

Sulfide probably plays an important role in removing Tl from anoxic waters in Siders Pond. A general negative correlation is found between Tl<sub>diss</sub> depletions and sulfide contents across all sampling days, and this is complemented by an opposing trend in the particulate data (Fig. 9). These trends are not surprising; Tl is a moderately chalcophile element with a known affinity for sulfide phases (summarized in Nielsen et al., 2017). The positive correlations found between Tlpart and the particulate abundances of Mo and Cd provide additional support for such a Tl-S link (Fig. 5). Molybdenum is rapidly removed from euxinic waters during the formation of highly particle-reactive thiomolybdate species  $(MoO_{4-x}S_x^{2-}; Erickson and Helz, 2000)$ , and formation of CdS (greenockite) under euxinic conditions is hypothesized to dramatically reduce Cd solubility (Rosenthal et al., 1995). A reasonable hypothesis is that, while biological uptake and sorption to Mn oxides help transfer Tl to anoxic waters, sulfide formation in these anoxic waters plays the more important role ultimately removing TI from the water column (and also sequestering TI in sediments; discussed below).

## 5.3. Thallium recorded in sediments

The goal of the leaching technique was to separate Tl bound to detrital minerals from authigenic Tl likely bound to sulfides (Nielsen et al., 2011). Only the latter fraction directly tracks changes in the low-T geochemical processes relevant to our study. With minor exception, the leaching technique seems to have effectively served its purpose. This is evident foremost by (a) the overlap between our  $\epsilon^{205}\text{Tl}_D$  values and average bulk upper continental crust, the likely source of detritus (Fig. 6C), and (b) distinguishably different  $\epsilon^{205}\text{Tl}_A$  values (Fig. 6A). Not surprisingly, the lone detrital sample that possesses a  $\epsilon^{205}\text{Tl}_D$  value lower than average bulk

upper continental crust ( $\epsilon^{205} Tl_A = -3.0 \pm 0.4$  at 8.5 m) is also the sample with an anomalously high authigenic Tl concentration ( $Tl_A = 1,548 \text{ ng/g}$ ), suggesting that some authigenic Tl was left behind in the solid detrital fraction of this sample after the leach. The fraction of total Tl extracted during the leach step is especially low in the samples collected at 2 m and 3 m ( $f_A = 0.28$  and 0.19, respectively; Fig. 6B). Conversely, but less definitively,  $\epsilon^{205} Tl_A$  values from these depths may be driven to slightly higher values due to partial extraction of some detrital Tl (e.g., Tl hosted in clays, biotite, or potassium feldspar).

With only minor exception, sediment  $\varepsilon^{205}$ Tl<sub>A</sub> values match estimated  $\epsilon^{205} Tl_{diss}$  values for average coeval waters in Siders Pond (Fig. 6A and Fig. 8F). Most likely, efficient transfer of Tl to sediments in association with sulfides facilitates  $\epsilon^{205} Tl_{diss}$  capture in this euxinic setting. Survival of the likely sulfide-driven particulate Tl-Mo-Cd links in these sediments supports this notion (Fig. 5B). Similar inferences have been invoked to explain capture of seawater  $\varepsilon^{205}$ Tl values in sediments below the oxycline in anoxic basins (Owens et al., 2017; Fan et al., 2020) and more recently in sediments formed below various upwelling zones (Wang et al., 2022b). Interestingly, however, and unlike in these other settings, capture of the water column  $\epsilon^{205}$ Tl value in Siders Pond sediments seems to occur despite extremely high sedimentary Mn enrichments in the sample collected closest to shore (up to  $Mn_{EF} = 199$ ; Fig. 6E). It may be that the types of Mn oxide minerals, if they are present in this sediment sample, are not ideal for driving large positive isotope fractionation effects. Such effects probably require Tl(I) oxidation (Schauble, 2007), a phenomenon observed thus far only after sorption to the highly-disordered phyllomanganate hexagonal birnessite (but not after sorption to triclinic birnessite or todorokite; Peacock and Moon, 2012).

Leached  $\varepsilon^{205}$ Tl<sub>A</sub> values from sediments collected immediately below the oxycline are slightly, yet consistently lower than predicted based on average water column salinity (4 m to 8.5 m water depth; Figs. 6A and 8F). We consider two possible explanations for these slightly lower  $\varepsilon^{205}$ Tl<sub>A</sub> values: (1) transfer of isotopically light biomass to sediments or (2) localized seawater influx. The lower  $\varepsilon^{205}$ Tl<sub>A</sub> values are accompanied by a peak in sedimentary Tl concentrations (Fig. 5B), an indication of particularly rapid Tl accumulation at these depths. If phytoplankton played a key role in removing isotopically light Tl from sunlit surface waters (see Section 5.1.2), then some of this light Tl could have been transferred to underlying sediments. Plankton remains have been implicated in previous work to help concentrate Tl in marine sediments formed off the coast of Peru (Böning et al., 2004). However, delivery of isotopically light biomass would presumably affect all depths below the oxycline within this very small body of water not just a select few immediately below the oxycline. Furthermore, core top sediments from highly productive upwelling regions of the ocean are not enriched in the lighter mass Tl isotope relative to seawater (Wang et al., 2022b). These sites would seem to be ideal for capture of an isotopically light biomass component, yet they seem unaffected. Perhaps because Tl in biomass is largely associated with the cytosol fraction in the cell (Zhang and Rickaby, 2020), efficient remineralization in the water column prevents delivery to and long-term burial within sediments. Or, at the least, remineralization prevents preservation of a sizable isotope fractionation effect in sediments (all data considered, the apparent sedimentary offset is small,  $\sim 1$  epsilon unit; Fig. 8).

Alternatively, and we argue more likely, seawater entering the pond at depth into sulfidic waters was near-quantitatively stripped of Tl, enriching sediments near this source in isotopically light Tl ( $\epsilon^{205}$ Tl<sub>seawater</sub> = -6.0 ± 0.3; Nielsen et al., 2006; Owens et al., 2017). Seawater input at depth has been invoked to explain the salinity stratification in Siders Pond (Caraco, 1986) and our sediment transects were conducted on the south side of the pond clos-

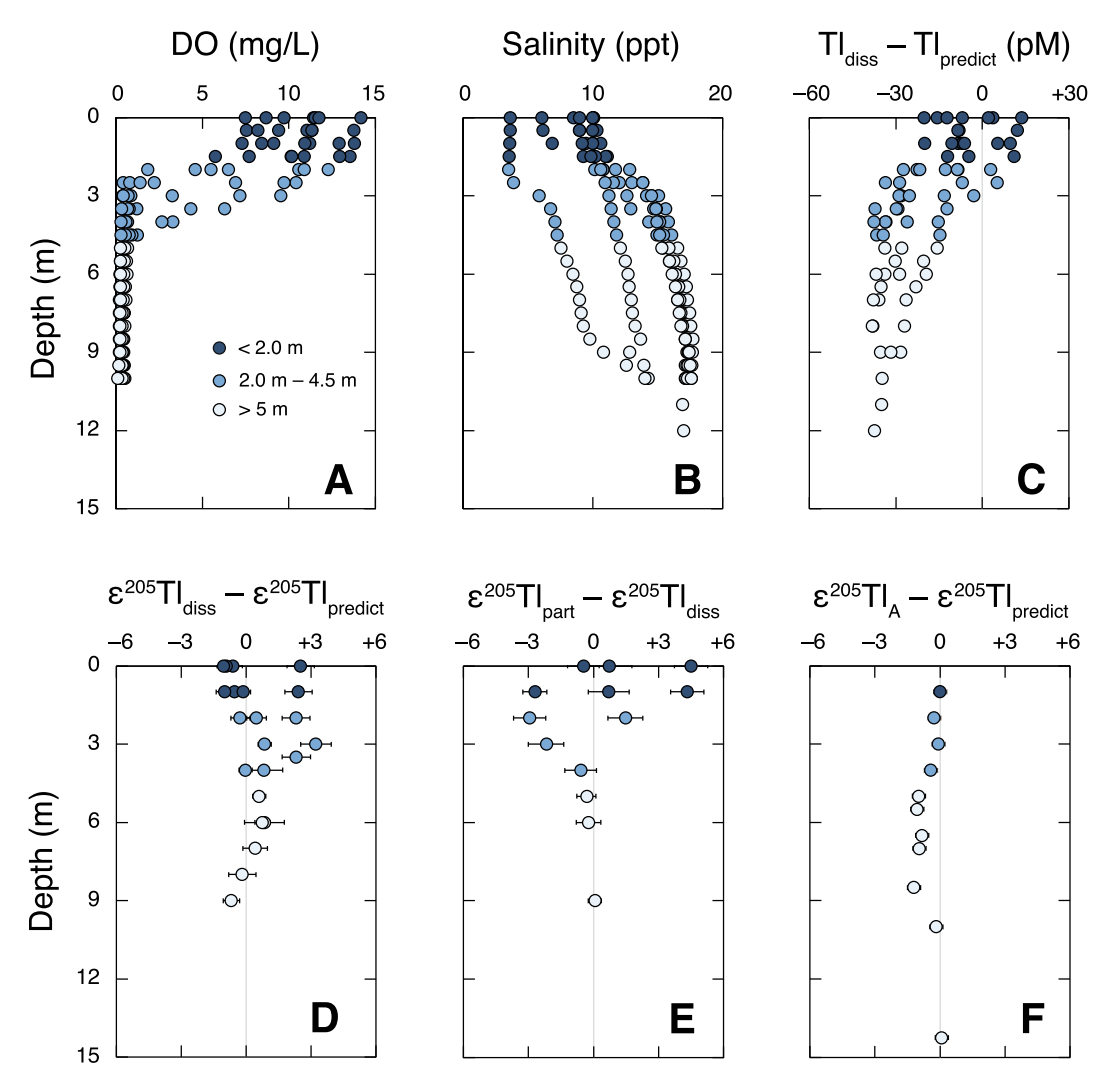


Fig. 8. Dissolved oxygen (A) and salinity (B) data collected during the three-year study. Datapoints in all panels are colored according to sample collection depth (see panel A legend). The calculated difference between measured TI abundances (C) and TI isotope compositions (D) on all sampling days and what is predicted based on two-component conservative mixing. (E) The calculated difference between particles and waters across all sampling days. (F) Calculated differences between authigenic TI isotope compositions and what are predicted for contemporaneous waters based on the average water column data.

est to Vineyard Sound - the proximal seawater source (Fig. 6D). Strong sedimentary Mo accumulation in coeval sediments (Fig. 5B) could also be consistent with this hypothesis because Mo is the most abundant transition metal in the ocean and gets rapidly removed from solution in the presence of sulfide (Erickson and Helz, 2000). The return to higher sedimentary  $\epsilon^{205} Tl_{\text{A}}$  values between 8.5 m and 10 m could simply be due to the fact that these samples were collected progressively further away from Vineyard Sound, and therefore also further away from any deep seawater source. Data collected from Siders Pond in 1982 shows that, while seawater input at depth had a strong impact on salinity at mid-depths, waters below 9 m were unaffected (Caraco, 1986). We observed the same general salinity mid-depth variability and deep stagnation between 2019 and 2021 (Figs. 2 and 3), supporting the notion that the deepest portion of the pond is not as strongly affected by seawater input below the oxycline.

## 5.4. Implications for the Tl isotope paleoredox proxy

The Siders Pond data have some important implications for the Tl isotope paleoredox proxy. Listed below are what we consider the three most important implications.

- The mere formation of Mn oxides in a water column seems insufficient to drive a substantial change in sedimentary  $\varepsilon^{205}$ Tl values. It has been hypothesized that, during the Archean Eon (4.0 to 2.5 billion years ago), Mn oxides may have been formed exclusively via anaerobic pathways in sunlit surface waters (via Mnoxidizing phototrophs (Johnson et al., 2013; Daye et al. 2019) or UV-light (Liu et al., 2020)). Yet, and irrespective of how Mn oxides are formed in Siders Pond surface waters, no net Tl isotope effect is imprinted on underlying anoxic sediments. It is only in sediments bathed under oxygenated waters, where Mn oxides are not just formed but presumably also buried, that any positive Tl isotope fractionation effect is registered (e.g., Rehkämper et al., 2002; Wang et al., 2022b). These findings support the use of Tl isotopes as a proxy uniquely capable of tracking Mn oxide burial, and hence O2 accumulation in marine bottom waters (e.g., Ostrander et al., 2019).
- Sediments formed throughout euxinic settings can be a robust archive of water column  $\varepsilon^{205}Tl$  values. In Siders Pond, we show that sediments formed above, within, and below the oxycline capture the adjacent water column  $\varepsilon^{205}Tl$  value (or nearly so). Moreover, particles delivered to and formed under these same (euxinic) conditions possess  $\varepsilon^{205}Tl$  values indistinguishable from coeval waters, even under non-quantitative Tl drawdown.

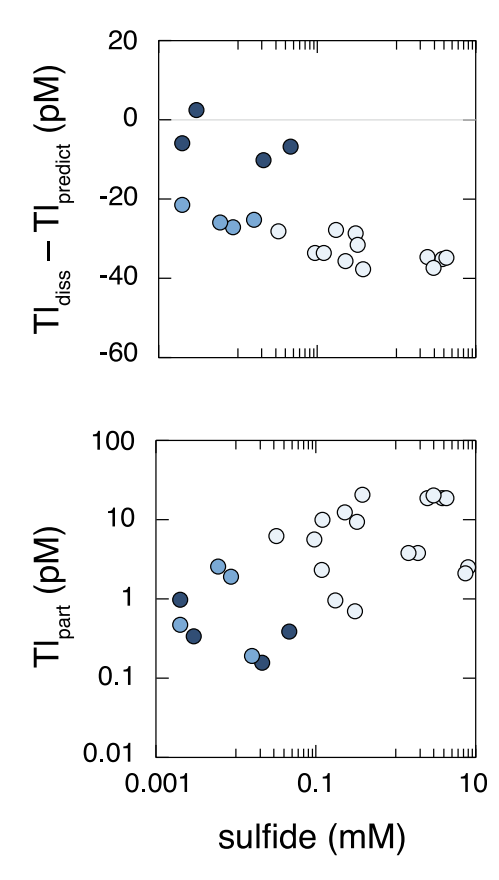


**Fig. 9.** Cross-plots showing (top) the apparent negative correlation connecting stronger Tl drawdown to higher sulfide contents and (bottom) the apparent positive correlation connecting higher Tl accumulation in particles to higher sulfide contents in Siders Pond. Datapoint color scheme is the same as in Fig. 8.

Altogether, these data suggest that the fractionation factor for Tl isotope fractionation into sulfides is small and that little to no Tl isotope fractionation takes place under euxinic conditions (see also Chen et al., 2022 for similar findings across the oxycline in the Black Sea).

• At least on short timescales, biology may play an as yet unrecognized role in driving water column and particle Tl isotope variability. A surprising finding of our three-year investigation was the preferential removal of the lighter-mass Tl isotope observed on some days in Siders Pond surface waters. For reasons discussed in Section 5.1.2., there is reason to think that biological Tl uptake plays some role in driving this effect. While this process clearly affects short-term Tl cycling (i.e., over days to weeks), no long-term effects from this process are clearly imprinted in pond sediments (i.e., over years).

#### 6. Conclusions

Between 2019 and 2021, we conducted a detailed Tl isotope investigation of Siders Pond, a salt-stratified body of water located on Cape Cod. Over short timeframes (i.e., days to weeks), we found that:

- Tl exhibits non-conservative behavior in surface waters, with episodes of Tl drawdown occurring more frequently than episodes of Tl accumulation;
- The lighter-mass Tl isotope (<sup>203</sup>Tl) was preferentially removed from the water column on days when Tl drawdown was especially strong, and we surmise that biological Tl uptake probably plays some role in this process;

- Preferential removal of the heavier-mass Tl isotope (<sup>205</sup>Tl) from surface waters was comparatively rare and occurred exclusively, and non-coincidentally, when particulate Mn oxide formation reached a three-year study high; and
- Below the oxycline in euxinic waters, Tl was rapidly removed from solution and transferred to particles and underlying sediments seemingly in association with sulfides and with no resolvable Tl isotope fractionation effect.

Data collected from sediments presumably speak to the longerterm Tl isotope cycle in Siders Pond (i.e., across years). According to these data:

• Minimal, if any, net Tl isotope fractionation takes place between waters and sediments in Siders Pond.

To summarize, although a large degree of dissolved and particulate Tl isotope variability is observed over short timescales in Siders Pond, only a small, nearly negligible amount of this variability gets preserved over longer timescales in the sedimentary record. In other words, limited net Tl isotope fractionation takes place in Siders Pond.

More work is warranted to address questions beyond the scope of our study. One example is to directly test the biological Tl uptake hypothesis and, if confirmed, try to better understand this process. More broadly, additional anoxic settings should be targeted to investigate similarities and differences across sites. One attractive target is anoxic and Fe(II)-rich (ferruginous) settings. Ferruginous conditions typified Precambrian oceans but are very rare today, and, hence, understudied (Swanner et al., 2020). Larger anoxic settings are another attractive target (e.g., the Baltic Sea, Kyllaren Fjord) more relatable to the open ocean anoxia experienced in deep time. The short-term dynamics observed in Siders Pond are largely an artifact of its small size and the relatively rapid changes in freshwater versus seawater inputs it experiences.

Notwithstanding, the results presented herein represent an important step forward in our understanding of the modern Tl cycle. Our findings provide new information about the mobility of Tl under different redox conditions, information that might prove useful in preventing or remediating the accumulation of this highly toxic element in nature. Our findings may corroborate the idea that biology plays a hitherto underappreciated role in the modern Tl cycle. And the results of our investigation, by bolstering our knowledge of the modern Tl isotope cycle, permit more confident inferences of this cycle in Earth's past.

## **Declaration of Competing Interest**

The authors declare that they have no known competing financial interests or personal relationships that could have appeared to influence the work reported in this paper.

## Acknowledgements

This work was supported financially by NSF-EAR 2129034 (to CMO, SGN, CMH), NSF-EAR2025853 (to CMH), NSF-OCE1736949 (to TJH), and a WHOI Postdoctoral Scholarship (to CMO). The MIT Department of Civil and Environmental Engineering provided financial support for HJG. We are thankful to the Siders Pond community for their hospitality and fervent interest, especially Paul and Joanne Skudder and the Falmouth Conservation Commission. We are thankful to (in alphabetical order) Maureen Auro, Sam Bowman, Kalina C. Grabb, Rachel Phillips, Lina Taenzer, and Logan A. Tegler for their assistance during pond monitoring, sampling, and sample processing. We thank Caroline Slomp for editorial han-

dling and Maya Gomes and two anonymous reviewers for thoughtful reviews of the original manuscript.

#### Appendix A. Supplementary material

All data reported in the current study are provided in Table S1. Supplementary material to this article can be found online at https://doi.org/10.1016/j.gca.2023.03.028.

#### References

- Ahrens, J., Beck, M., Böning, P., Degenhardt, J., Pahnke, K., Schnetger, B., Brumsack, H., 2021. Thallium cycling in pore waters of intertidal beach sediments. Geochim. Cosmochim. Acta 306, 321–339.
- Altmann, H.J., 1972. Bestimmung von in Wasser gelöstem Sauerstoff mit Leukoberbelinblau I Eine Schnelle Winkler-Methode. Fresenius' Zeitschrift für Analytische Chemie 262, 97–99.
- Bishop, J.K.B., Lam, P.J., Wood, T.J., 2012. Getting good particles: accurate sampling of particles by large volume in-situ filtration. Limnol. Oceanogr. Methods 10, 681–710
- Böning, P., Brumsack, H.J., Böttcher, M.E., Schnetger, B., Kriete, C., Kallmeyer, J., Borchers, S.L., 2004. Geochemistry of Peruvian near-surface sediments. Geochim. Cosmochim. Acta 68, 4429–4451.
- Böning, P., Schnetger, B., Beck, M., Brumsack, H.J., 2018. Thallium dynamics in the southern North Sea. Geochim. Cosmochim. Acta 227, 143–155.
- Calvert, S.E., Pedersen, T.F., 1996. Sedimentary geochemistry of manganese: Implications for the environment of formation of manganiferous black shales. Econ. Geol. 91, 36–47.
- Caraco, N., 1986. Phosphorous, iron, and carbon cycling in a salt stratified coastal pond. PhD. Dissertation. Boston University, 213 p.
- Chen, X., Li, S., Newby, S.M., Lyons, T.W., Wu, F., Owens, J.D., 2022. Iron and manganese shuttle has no effect on sedimentary thallium and vanadium isotope signatures in Black Sea sediments. Geochim. Cosmochim. Acta 317, 218–233.
- Cutter, G., Casciotti, K., Croot, P., Geibert, W., Heimbürger, L.E., Lohan, M., Planquette, H., van de Flierdt, T., 2017. Sampling and sample-handling protocols for GEOTRACES cruises. GEOTRACES.
- Daye, M., Klepac-Ceraj, V., Pajusalu, M., Rowland, S., Farrell-Sherman, A., Beukes, N., Tamura, N., Fournier, G., Bosak, T., 2019. Light-driven anaerobic microbial oxidation of manganese. Nature 576, 311–314.
- Erickson, B.E., Helz, G.R., 2000. Molybdenum (VI) speciation in sulfidic waters: stability and lability of thiomolybdates. Geochim. Cosmochim. Acta 64, 1149–1158
- Fan, H., Nielsen, S.G., Owens, J.D., Auro, M., Shu, Y., Hardisty, D.S., Horner, T.J., Bowman, C.N., Young, S.A., Wen, H., 2020. Constraining oceanic oxygenation during the Shuram excursion in South China using thallium isotopes. Geobiology 18, 348–365.
- Flegal, A.R., Patterson, C.C., 1985. Thallium concentrations in seawater. Mar. Chem. 15, 327–331.
- Froelich, P.N., Klinkhammer, G.P., Bender, M.L., Luedtke, N.A., Heath, G.R., Cullen, D., Dauphin, P., Hammond, D., Hartman, B., Maynard, V., 1979. Early oxidation of organic matter in pelagic sediments of the eastern equatorial Atlantic: suboxic diagenesis. Geochim. Cosmochim. Acta 43, 1075–1090.
- Gadol, H.J., 2021. Cycling of iron and manganese (oxyhydr)oxides in the presence of organic matter. Massachusetts Institute of Technology, Cambridge, Massachusetts.
- Hein, J.R., Koschinsky, A., 2014. Deep-ocean ferromanganese crusts and nodules. In: Scott, S. (Ed), Treatise on Geochemistry 2<sup>nd</sup> Edition (TGC2), New Volume on Geochemistry of Mineral Deposits, 2<sup>nd</sup> ed. Pp. 273–291.
- Jochum, K.P., Weis, U., Schwager, B., Stoll, B., Wilson, S.A., Haug, G.H., Andreae, M.O., Enzweiler, J., 2016. Reference values following ISO guidelines for frequently requested rock reference materials. Geostand. Geoanal. Res. 40, 333–350.
- Johnson, J.E., Webb, S.M., Thomas, K., Ono, S., Kirschvink, J.L., Fischer, W.W., 2013. Manganese-oxidizing photosynthesis before the rise of cyanobacteria. Proc. Natl. Acad. Sci. U.S.A. 110, 11238–11243.
- Liu, W., Hao, J., Elzinga, E.J., Piotrowiak, P., Nanda, V., Yee, N., Falkowski, P.G., 2020. Anoxic photogeochemical oxidation of manganese carbonate yields manganese oxide. Proc. Natl. Acad. Sci. U.S.A. 117, 22698–22704.
- Lyons, T.W., Diamond, C.W., Planavsky, N.J., Reinhard, C.T., Li, C., 2021. Oxygenation, life, and the planetary system during Earth's middle history: an overview. Astrobiology 21, 906–923.
- Madison, A.S., Tebo, B.M., Mucci, A., Sundby, B., Luther III, G.W., 2013. Abundant porewater Mn(III) is a major component of the sedimentary redox system. Science 341, 875–878.
- Mori, C., Beck, M., Striebel, M., Merder, J., Schnetger, B., Dittmar, T., Pahnke, K., Brumsack, H., 2021a. Biogeochemical cycling of molybdenum and thallium

- during a phytoplankton summer bloom: A mesocosm study. Mar. Chem. 229, 103910
- Mori, C., Beck, M., Hintz, N.H., Merder, J., Bunse, C., Dittmar, T., Klugosch, L., Böttcher, L., Pahnke, K., Striebel, M., Schnetger, B., Simon, M., Brumsack, H., 2021b. Biogeochemical thallium cycling during a mesocosm phytoplankton spring bloom: biotic versus abiotic drivers. Geochim. Cosmochim. Acta 313, 257–276.
- Nielsen, S.G., Rehkämper, M., Baker, J.A., Halliday, A.N., 2004. The precise and accurate determination of thallium isotope compositions and concentrations for water samples by MC-ICPMS. Chem. Geol. 204, 109–124.
- Nielsen, S.G., Rehkämper, M., Teagle, D.A.H., Butterfield, D.A., Alt, J.C., Halliday, A.N., 2006. Hydrothermal fluid fluxes calculated from the isotopic mass balance of thallium in the ocean crust. Earth Planet. Sci. Lett. 251, 120–133.
- Nielsen, S.G., Rehkämper, M., Brandon, A.D., Norman, M.D., Turner, S., O'Reilly, S.Y., 2007. Thallium isotopes in Iceland and Azores lavas—implications for the role of altered crust and mantle geochemistry. Earth Planet. Sci. Lett. 264, 332–345.
- Nielsen, S.G., Goff, M., Hesselbo, S.P., Jenkyns, H.C., LaRowe, D.E., Lee, C.A., 2011. Thallium isotopes in early diagenetic pyrite – A paleoredox proxy? Geochim. Cosmochim. Acta 75, 6690–6704.
- Nielsen, S.G., Wasylenki, L.E., Rehkämper, M., Peacock, C.L., Xue, Z., Moon, E.M., 2013. Towards an understanding of thallium isotope fractionation during adsorption to manganese oxides. Geochim. Cosmochim. Acta 117, 252–265.
- Nielsen, S.G., Klein, F., Kading, T., Blusztajn, J., Wickham, K., 2015. Thallium as a tracer of fluid-rock interaction in the shallow Mariana forearc. Earth Planet. Sci. Lett. 430, 416–426.
- Nielsen, S.G., Rehkämper, M., Prytulak, J., 2017. Investigation and application of thallium isotope fractionation. Rev. Mineral. Geochem. 82, 759–798.
- Oldham, V.E., Owings, S.M., Jones, M.R., Tebo, B.M., Luther, G.W., 2015. Evidence for the presence of strong Mn(III)-binding ligands in the water column of the Chesapeake Bay. Mar. Chem. 171, 58–66.
- Ostrander, C.M., Owens, J.D., Nielsen, S.G., 2017. Constraining the rate of oceanic deoxygenation leading up to a Cretaceous Oceanic Anoxic Event (OAE-2: ~94 Ma). Sci. Adv. 3, e1701020.
- Ostrander, C.M., Nielsen, S.G., Owens, J.D., Kendall, B., Gordon, G.W., Romaniello, S.J., Anbar, A.D., 2019. Fully oxygenated water columns over continental shelves before the Great Oxidation Event. Nat. Geosci. 12, 186–191.
- Owens, J.D., Nielsen, S.G., Horner, T.J., Ostrander, C.M., Peterson, L.C., 2017. Thallium-isotopic compositions of euxinic sediments as a proxy for global manganese-oxide burial. Geochim. Cosmochim. Acta 213, 291–307.
- Peacock, C.L., Moon, E.M., 2012. Oxidative scavenging of thallium by birnessite: explanation for thallium enrichment and stable isotope fractionation in marine ferromanganese precipitates. Geochim. Cosmochim. Acta 84, 297–313.
- Rehkämper, M., Frank, M., Hein, J.R., Porcelli, D., Halliday, A., Ingri, J., Liebetrau, V., 2002. Thallium isotope variations in seawater and hydrogenetic, diagenetic, and hydrothermal ferromanganese deposits. Earth Planet. Sci. Lett. 197, 65–81.
- Rehkämper, M., Halliday, A.N., 1999. The precise measurement of TI isotopic compositions by MC-ICPMS: application to the analysis of geologic materials and meteorites. Geochim. Cosmochim. Acta 63, 935–944.
- Rosenthal, Y., Lam, P., Boyle, E.A., Thomson, J., 1995. Authigenic cadmium enrichments in suboxic sediments: precipitation and postdepositional mobility. Earth Planet. Sci. Lett. 132, 99–111.
- Rudnick, R.L., Gao, S., 2003. Composition of the continental crust. In: Rudnick, R.L. (Ed.). The Crust. Elsevier. Amsterdam. pp. 1–64.
- Schauble, E.A., 2007. Role of nuclear volume in driving equilibrium stable isotope fractionation of mercury, thallium, and other very heavy elements. Geochim. Cosmochim. Acta 71, 2170–2189.
- Shu, Y., Nielsen, S.G., Zeng, Z., Shinjo, R., Blusztajn, J., Wang, X., Chen, S., 2017. Tracing subducted sediment inputs to the Ryukyu arc-Okinawa trough system: Evidence from thallium isotopes. Geochim. Cosmochim. Acta 217, 462–491.
- Swanner, E.D., Lambrecht, N., Wittkop, C., Harding, C., Katsev, S., Torgeson, J., Poulton, S.W., 2020. The biogeochemistry of ferruginous lakes and past ferruginous oceans. Earth Sci. Rev. 211, 103430.
- Tao, Z., Gameiro, A., Grewer, C., 2008. Thallium ions can replace both sodium and potassium ions in the glutamate transporter EAAC1. Biochemistry 47, 12923– 12930.
- Them, T.R., Gill, B.C., Caruthers, A.H., Gerhardt, A.M., Gröcke, D.R., Lyons, T.W., Marroquin, S.M., Nielsen, S.G., Trabucho Alexandre, J.P., Owens, J.D., 2018. Thallium isotopes reveal protracted anoxia during the Toarcian (Early Jurassic) associated with volcanism, carbon burial, and mass extinction. Proc. Natl. Acad. Sci. U.S.A. 115, 6596–6601.
- Wang, Y., Bodin, S., Blusztajn, J.S., Ullmann, C., Nielsen, S.G., 2022a. Orbitally paced global oceanic deoxygenation decoupled from volcanic CO<sub>2</sub> emission during the middle Cretaceous Oceanic Anoxic Event 1b (Aptian-Albian transition). Geology 50, 1324–1328.
- Wang, Y., Lu, W., Costa, K.M., Nielsen, S.G., 2022b. Beyond anoxia: exploring sedimentary thallium isotopes in paleo-redox reconstructions from a new core top collection. Geochim. Cosmochim. Acta 333, 347–361.
- Zhang, Q., Rickaby, R.E.M., 2020. Interactions of thallium with marine phytoplankton. Geochim. Cosmochim. Acta 276, 1–13.
- Zitko, V., 1975. Toxicity and pollution potential of thallium. Sci. Total Environ. 4, 185–192.